Mon. Not. R. Astron. Soc. **337,** 1233–1244 (2002)

Simulations of central structure in barred galaxies

P. Rautiainen,⋆ H. Salo and E. Laurikainen
University of Oulu, Department of Physical Sciences, Astronomy Division, PO Box 3000, FIN-90014 Oulun yliopisto, Finland

Accepted 2002 August 6. Received 2002 July 26; in original form 2002 February 6

ABSTRACT

We have studied the formation of complex central structures in barred galaxies – nested bars, nuclear spirals and circumnuclear rings – by making *N*-body simulations, which include the gas component as inelastically colliding particles. Our models suggest that many of the observed features in both the stellar and gas components can be explained by the dynamical effect of two or more modes in the stellar disc. Especially, many morphological features in our simulations correspond to analytically studied orbit loops in double-barred potentials. Interestingly, a fast-rotating secondary bar forms in a purely stellar disc in our simulations, which disagrees with some previous studies where the presence of a dissipative component was needed.

Key words: galaxies: evolution – galaxies: fundamental parameters – galaxies: kinematics and dynamics – galaxies: spiral – galaxies: structure.

1 INTRODUCTION

Many galaxies have complex central morphology inside a radius of one or two kpc from the nucleus. Most of the known cases have been detected quite recently (see e.g. Wozniak et al. 1995; Friedli et al. 1996; Carollo et al. 1997). Only a few examples such as NGC 1097 (Burbidge & Burbidge 1960) and NGC 4314 (Sandage 1961) were known before the era of CCD detectors. The observed nuclear features have a large variety from secondary bars to nuclear spirals and ring structures. Just as the outer and inner pseudorings can be composed of tightly wound spiral arms (Buta & Combes 1996), there are also corresponding examples in the nuclear features. The composition of the nuclear structures varies from mainly gaseous features to ones with the main contribution from the old stellar population. There are often signs of enhanced star formation in the nuclear rings (Buta & Combes 1996), and the observed nuclear morphology may depend on the wavelength used. For example, in ESO 565-11 the star clusters form a nuclear ring, whereas the dust forms spiral arms (Buta, Crocker & Byrd 1999).

There are several possible physical mechanisms for the generation of the central structures. For example, a rotating stellar bar can induce resonances in the disc, e.g. a nuclear ring can form near the inner Lindblad resonance (ILR) (Buta & Combes 1996). Heller, Shlosman & Englmaier (2001) proposed that a gaseous double nuclear ring (close to two ILRs) could have a hydrodynamic instability leading to a very elongated nuclear ring or secondary bar, with lower pattern speed than the primary bar. It has also been proposed that a spiral-shaped nuclear feature reaching inside the ILR radius could form owing to the gas response to the rotating background gravitational potential of the disc provided by a large stellar bar (Englmaier & Shlosman 2000; Maciejewski et al. 2002).

⋆E-mail: pertti.rautiainen@oulu.fi

Periodic orbits have been a backbone to many studies of the dynamics of barred galaxies. For example, the x_1 orbit family (Contopoulos & Grosbol 1989) supports the bar itself, and the perpendicularly aligned x_2 family is often identified with the nuclear ring. However, many barred galaxies have a misaligned secondary bar, the pattern speed of which is probably different from that of the primary bar, most likely higher (Friedli & Martinet 1993). This means that, at least in certain regions, the studies assuming a single pattern speed fail to give a complete description of the actual orbital structures.

Maciejewski & Sparke (1997, 2000) have recently studied analytical potential models for double-barred galaxies, and have introduced a generalization to periodic orbits found in single bar potential: loops. The shape of the loop changes cyclically depending on the relative orientation of the two bars. Although the shape of the loop is the same in similar alignments of the bars, a particle belonging to a loop does not return to its original position after one loop period. Maciejewski & Sparke found loops that can support the double bar structure. The x_1 loops, which are counterparts for the x_1 orbits in single bar potentials, support the primary bar. The x_2 loops, which correspond to the x_2 orbits of the single bar case, exhibit radial dependence in their shape and orientation: the outermost x_2 loops follow the rotation of the primary bar, while the innermost ones support the secondary bar. Interestingly, when defined by the supporting orbits, the secondary bar is hollow, i.e. the x_2 loops do not extend to the nucleus, but there is an inner population of x_1 loops, the major axis of which is always close to parallel alignment with the primary bar. Note that in a single bar potential with two ILRs, the innermost orbits also tend to be aligned parallel with the main bar.

In our previous *N*-body simulation studies we have paid attention to large-scale morphology of barred galaxies: the connection between bars and spiral arms (Rautiainen & Salo 1999, hereafter

Paper I) and the formation of rings in models with both steadily rotating bar potential (Byrd et al. 1994; Salo et al. 1999) and a self-gravitating stellar bar (Rautiainen & Salo 2000, hereafter Paper II). We now focus on nuclear regions of barred galaxies and show a few new examples of *N*-body simulations exhibiting multiple-mode phenomena, some of which can be explained by loops previously studied by analytical models.

This article is organized as follows. In Section 2 we briefly describe the simulation program and the analysis methods. In Section 3 examples exhibiting various nuclear features are presented and in Section 4 we discuss how our results are related to observations and recently published models. Finally, we present our conclusions in Section 5.

2 METHODS

We have studied the dynamics of barred galaxies by performing both two- and three-dimensional *N*-body simulations. The three-dimensional simulations are necessary to decrease the value of the gravity softening parameter, which in two-dimensional models acts also as a correction for a finite thickness of the disc (Sellwood 1987). To have high resolution in the central region, we apply a logarithmic polar grid, or a spherical polar grid in the three-dimensional case (see Salo 1991a; Salo & Laurikainen 1993, 2000a), to calculate the gravity potential. In two-dimensional simulations the grid geometry is 108 azimuthal and 144 radial cells, whereas in three-dimensional models the grid is sparser with 72 azimuthal and radial cells, and 37 latitudinal cells, in which case the vertical resolution corresponds to the resolution in the disc plane. Thus, at 1 kpc radius the grid softening ϵ_g is approximately 60 pc in the two-dimensional models and about 90 pc in three-dimensional models. Both values are smaller than the used gravity softening ϵ, which is 375 pc in two-dimensional models and 150 pc in three-dimensional models. In all simulations the central hole of the gravity grid is much smaller (37.5 pc in two-dimensional models and 60 pc in three-dimensional models) than the studied physical structures. At the region covered by the grid, we calculated the gravitational potential with the Fast Fourier Transform (FFT) over azimuthal direction, combined with direct summation over the grid cells in the radial and vertical directions. The particle orbits are also accurately integrated in the grid hole region using forces obtained by direct summation over the grid. Time integrations are performed with a Cartesian time-centred leapfrog method. The time step is chosen in such a manner that at least 40 steps per orbit are used even in the innermost parts.

The initial stellar disc has an exponential particle distribution. In all cases we scale our results so that the initial scalelength of the disc is 3 kpc. In two-dimensional and three-dimensional models we use 500 000 and 2 million stellar particles, respectively. In addition to stars, our models include gas with different initial distributions. In Model I, to highlight the nuclear features in Model I, we have put all the particles inside 4.5 kpc (uniform surface density to 3 kpc and gradual decline to zero at 4.5 kpc). In models II and III the initial gas distribution reaches larger radius, because we are also interested in the effect of gas inflow (the nuclear morphology of Model I is essentially the same even when the initial gas distribution reaches the edge of the stellar disc). Model II has uniform gas surface density inside 15 kpc (gradual decline to zero at 18 kpc) and Model III has an exponential distribution with a scalelength of 6.75 kpc and cut-off radius at two scalelengths. The most important model parameters are shown in Table 1.

Table 1. Basic information about the models. The listed parameters are disc mass M_D, bulge mass M_B, halo mass M_H (in units of $10^{10}\,M_\odot$), the length-scale of the bulge (in kpc), Toomre parameter Q_T and the value of the softening parameter ϵ (in kpc).

Model	M_D	M_B	M_H	r_B	Q_T	ϵ
Model I	7.5	1.6	0.0	0.6	1.75	0.375
Model II	7.5	0.3	0.0	0.3	1.5	0.15
Model III	7.5	0.3	0.0	0.3	1.5	0.15
Model IV	4.8	1.6	6.0	0.6	1.25	0.15

The gas component is modelled as 40 000 inelastically colliding particles ('sticky particle method'). In each collision, the relative velocity component in the direction of the line joining the particle centres is reversed and multiplied by the coefficient of restitution, α, typically either 0.0 or 0.5. On the other hand, the tangential relative velocity component (in the plane perpendicular to the line joining the particle centres) is not changed, so that the total loss of random kinetic energy in each impact amounts to

$$\frac{1}{4}(1-\alpha^2)(\Delta \boldsymbol{v}\cdot\boldsymbol{c})^2,$$

where $\Delta \boldsymbol{v}$ is the precollisional relative velocity and $\boldsymbol{c}$ is the unit vector in the direction joining the particle centres. The treatment of impacts is made by methods typically employed in planetary ring simulations (Salo 1991b, 1992). We have made simulations both with massless and self-gravitating gas particles. The velocity dispersion of the gas varies from 2 to 30 km s^{-1}. We employ particle radius $r_g = 0.75$ pc in two-dimensional Model I, and three-dimensional models II and III $r_g = 15$ pc.

The radius of a gas particle r_g in our simulations should not be thought of as representing the radius of an actual gas cloud, but as more like a parameter to control the amount of dissipation, via the frequency of collisions between particles. In general, the impact frequency ω_c is proportional to the geometric optical depth of gas particles, $\tau = \pi r_g^2 n_g$, where n_g is the surface number density. There are some problems, which are difficult to avoid when using finite-sized particles to represent gas. For example, if the particles are very small, two crossing 'gas streams' may cross each other without hindrance by a shock. This is the case if the average interval between impacts experienced by a particle, is larger than the dynamical time-scale. On the other extreme, a too large particle size can limit the maximal amount the gas component can 'compress', owing to the finite size required by particles. Since during the course of the simulation the gas component develops rather large density variations, i.e. ranging from those corresponding to dense nuclear rings to the rather sparse outer disc regions, considerable care is needed in choosing a meaningful r_g. In practice, with our adopted values for r_g and the number of gas particles, the initial geometrical depth τ (at 1 kpc from the centre) is in the range 0.002–0.05, so that when ring structures form the collision frequency exceeds several impacts per orbital revolution.

An additional technical problem related to high collision frequency is the slowing down of the calculation of impacts. In principle, our method attempts to find the exact locations of all impacts between particles, as is done in planetary ring simulations, by taking into account the changes of the orbits of colliding particles in determination of their subsequent impacts during the time step studied (see Salo 1991a). Since this leads to an excessive CPU time consumption in cases where extremely high densities develop, in practice we have limited the impact frequency to one

impact/particle/time-step. This inevitably leads to missing a fraction of impacts and thus to overlapping particle pairs. To minimize the number of overlapping particles, and also to speed up the calculations in general, a simple scheme of removing gas particles from high density regions was adopted. Thus, in each collision there is a small probability (typically 0.05 per cent) for a gas cloud to be transformed in to a non-colliding stellar particle. In some sense this method could be considered as a crude way of mimicking gas consumption related to star formation. The method works fine in Model I, but is less successful in models II and III, which have higher gas density, and thus exhibit some regions where particles are overpacked.

The exact consequences of particle overlapping is difficult to examine, since any attempt to cure it will simultaneously affect the dissipation rate of the system. Therefore, we have typically made several variations of our simulation models with slightly different gas particle properties, and discuss the indicated changes.

In addition to morphological analysis of the stellar and gas components of the models, Fourier analysis of the disc surface density has been made. This was done in two stages. First, we made a Fourier decomposition of surface density at different time-steps, including azimuthal Fourier components up to $m = 4$. From the individual decompositions amplitude spectra were constructed showing amplitudes at different pattern speeds and distances (see Masset & Tagger 1997; Rautiainen & Salo 2000; Salo & Laurikainen 2000b). The amplitude spectra were plotted with curves showing Ω, $\Omega - \kappa/2$ and $\Omega - \kappa/4$ (here Ω is the local circular frequency and κ is the epicycle frequency) to estimate the possible resonances related to modes in stellar and gas discs.

3 CASE STUDIES

Here we show examples exhibiting various nuclear features and analyse these cases thoroughly. These models were chosen to demonstrate the diversity of the nuclear morphology seen in simulations: secondary bars, double nuclear rings and nuclear spirals. Thus, our models do not form a series of systematically changing parameter values as was the case in Papers I and II. The basic parameters of our four models are shown in Table 1.

3.1 Model I

Our first example is a two-dimensional model showing both a primary bar and a secondary bar. The model has an analytical Plummer bulge with a mass of 1.6×10^{10} $M_\odot$ and scale radius of 0.6 kpc, and a self-gravitating two-dimensional exponential disc whose mass is 7.5×10^{10} $M_\odot$, resulting to maximal rotation velocity of about 225 km s^{-1} (taking into account the softening). There is no halo component. The initial value of the Toomre parameter Q_T is 1.75, thus the model is the same as Model A1.75 in Paper II. The value of the coefficient of restitution is 0.5.

Although the large-scale bar develops quickly (at $T \approx 1$ Gyr) it is preceded by the secondary bar ($T \approx 0.7$ Gyr). From the $m = 2$ amplitude spectrum of Fig. 1 we can see that these are two modes with different pattern speeds: the secondary bar rotates almost four times faster than the primary bar. The amplitude spectrum suggests that the two bars are in CR–ILR mode coupling because the ILR radius of the primary bar is close to corotation of the secondary bar (Tagger et al. 1987; Masset & Tagger 1997). Note however, that these radii are based on the linear approximation, which is not valid when the bar is strong as in this case. The secondary bar is short: it ends at about 1.5 kpc, well before reaching its corotation radius (about 3.1 kpc) or even inner 4/1-radius (about 2.1 kpc). Furthermore, it is also clear that the secondary bar mode does not reach the nucleus: the central region is rather dominated by the primary bar mode. This is the situation that would be expected in the case of loops: the secondary bar is supported by particles around inner x_2 loops and it is hollow because the innermost region is dominated by x_1 loops (Maciejewski & Sparke 2000).

In Fig. 2 we show the stellar morphology of Model I in selected time-steps as isodensity contours of the $m = 2$ Fourier component of the disc surface density. The secondary bar is seen here as two distinctive blobs (pointed by arrows in Fig. 2), while in direct images it has often a vaguely spiral shape. Spiral-like features (both trailing and leading) can be seen also in the $m = 2$ isodensity contours, usually connecting features with different pattern speeds. The secondary bar rotates steadily for several Gyr and the major axis of the gaseous nuclear ring is usually parallel to it (the gas ring is shown only in the sixth frame). Inside the nuclear ring and secondary bar, there is a short bar-like component (two innermost blobs in Fig. 2),

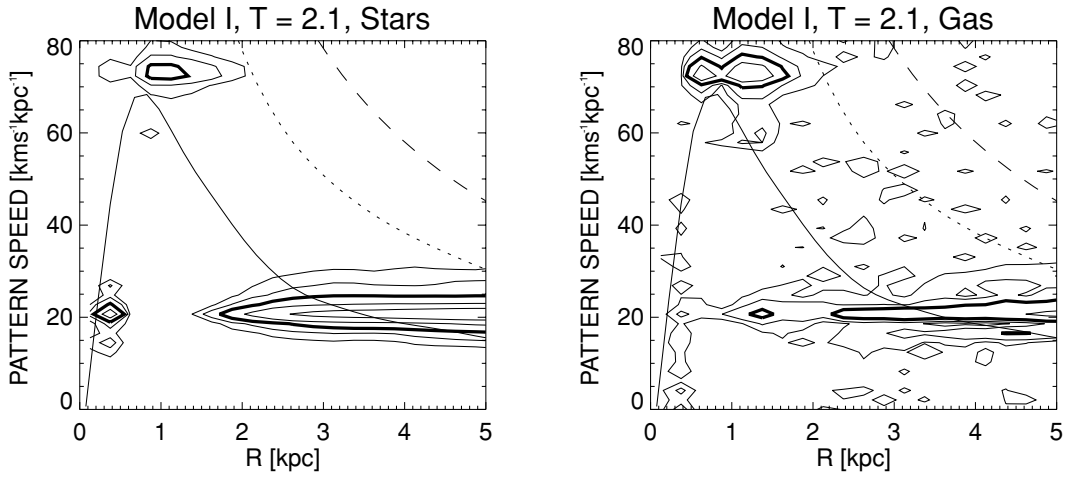

Figure 1. The amplitude spectra of the $m = 2$ density component normalized to the $m = 0$ component in a double-barred Model I. For the stellar component (left frame) the contour levels are 0.025, 0.05, 0.1 (thick line), 0.2 and 0.4. For the the gas component (right frame) the levels are three times those of the stellar component. The time interval used in the construction of the amplitude spectra is 1.5 Gyr centred at $T = 2.1$ Gyr. The continuous curve shows $\Omega - \kappa/2$, the dotted curve $\Omega - \kappa/4$ and the dashed curve Ω.

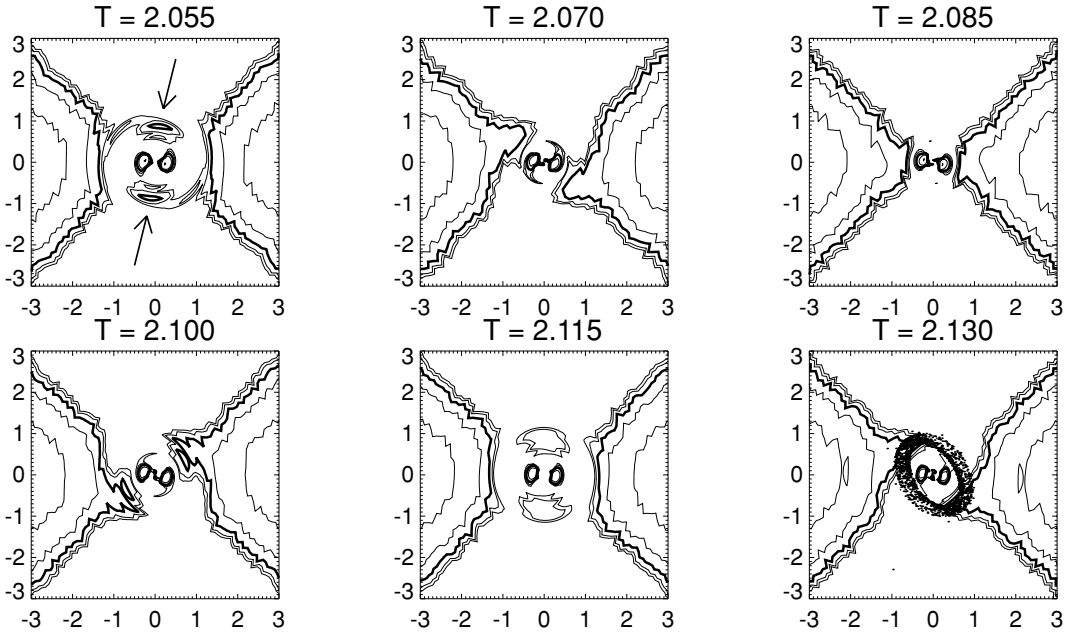

Figure 2. The rotation of the secondary bar in Model I. The isodensity contours of the $m = 2$ Fourier component of the stellar surface density are shown. The primary bar (mostly outside the frames) is horizontal. The contour levels are the same as in Fig. 1 and the time is shown in Gyr. The feature identified as secondary bar is indicated by arrows in the first frame, and the gaseous nuclear ring is overplotted in the last frame.

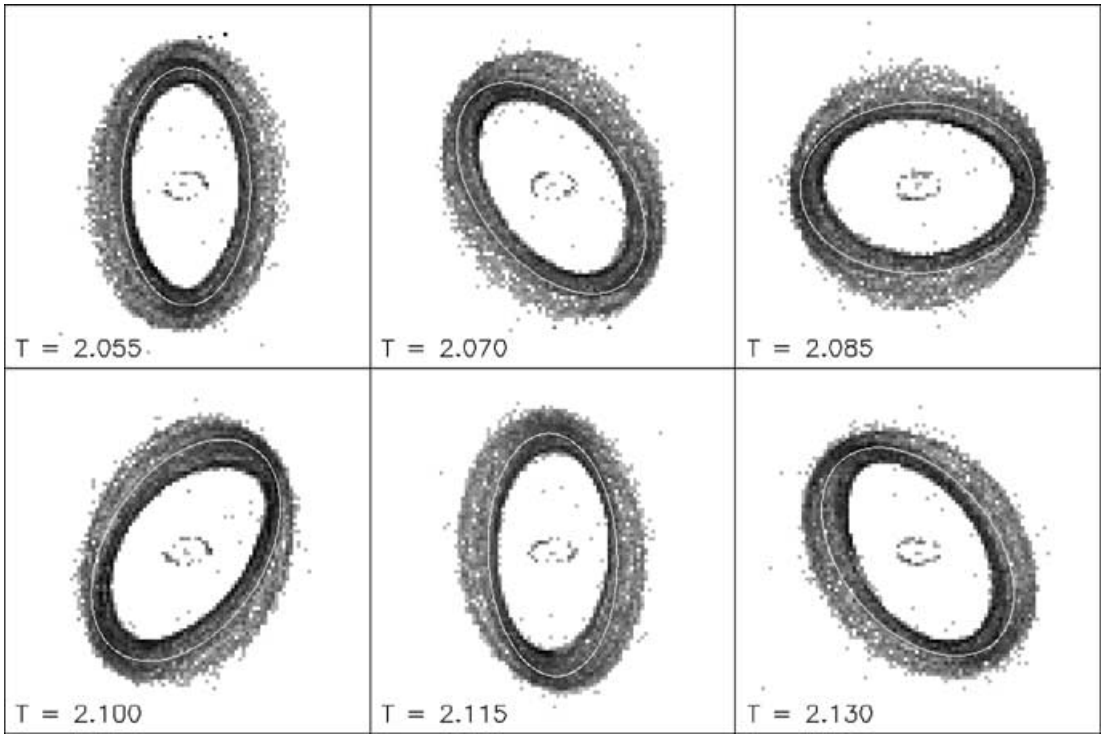

Figure 3. The evolution of the shape of the gaseous nuclear ring in Model I. The result of automatic ellipse fitting is shown as a white line. The width of the frame is 3 kpc. The time-steps are the same as in Fig. 2, with the primary bar aligned horizontally.

which is almost parallel to the primary bar. This, together with the amplitude spectrum, agrees strongly with the presence of loops.

The clearest evidence for inner x_2 loops can be seen in the cyclic evolution of the shape of the gaseous nuclear ring. In Fig. 3 we show how the shape of such a nuclear ring depends on the relative alignment of the two bars. We have also performed an automatic ellipse fitting to the gas density. The fitted ellipses are plotted over the gas distribution in Fig. 3, and in Fig. 4 we show the collected fitting results. One can easily see both from the density plots and from the ellipse fitting results that the minor-to-major axis ratio of

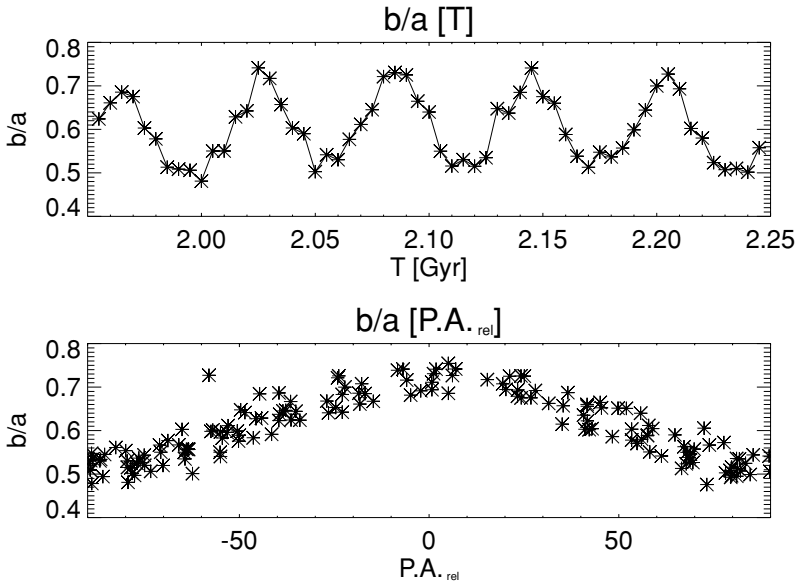

Figure 4. The result of ellipse fitting to the nuclear ring seen in Fig. 3. The top frame shows the minor-to-major axis ratio as a function of time. The bottom frame shows the minor-to-major axis ratio as function of the position angle between the major axes of the secondary and the primary bar. The time interval is longer in the bottom frame, $T = 1.8$–3.6 Gyr. The resolution is increased by putting all the gas particles initially inside 4.5 kpc.

the ring clearly depends on the relative position angle of the secondary bar with respect to the primary bar: the ring is roundest when the bars are parallel and most eccentric when the bars are perpendicularly aligned. There is also another, smaller nuclear ring which is aligned parallel with respect to the primary bar. These rings and their behaviour corresponds exactly the loops found by Maciejewski & Sparke (2000) in their analytical bar models. In addition, the larger nuclear ring is not actually ellipse-shaped. It is rather broad, and if one fits ellipses separately to the inner and the outer edge of the ring, one can easily see that there is a twist between the major axes (see gas distribution at $T = 2.1$ Gyr in Fig. 3). This twist, which depends on the relative alignment of the two bars, resembles the orientation differences between loops in fig. 6 in Maciejewski & Sparke (2000), and can be considered as further evidence for orbit loops.

Model I is not the only one of our models showing cyclically evolving nuclear morphology, but it is the one with the most elongated nuclear ring. Furthermore, this phase is long-lived (lasts more than 4 Gyr until the end of the simulation), therefore being a well suited model for demonstrating this kind of behaviour. However, also short-lived nuclear rings and bars appear in our simulations.

The young nuclear ring in Model I has several blobs that disperse, sometimes forming short spiral arcs in the ring. Later, the ring becomes smoother, smaller and more elongated. The gas amplitude spectrum of Fig. 1 is from a model with a uniform initial gas distribution inside five scalelengths of the stellar disc. Because gas is massless, we could get more resolution in the centre by putting all the gas particles initially inside 4.5 kpc. Furthermore, we have included the simple star formation mechanism (see Section 2) to avoid particle overpacking. This is efficient: neglecting a few randomly distributed occasions, there are essentially no overlapping particles in this model. To test how our results depend on the amount of dissipation, we have made several variations of Model I by changing the gas parameters. With even 50 times larger particle size, and the star formation procedure inhibited, the cyclic behaviour of the larger nuclear ring is very much the same as in the basic case, although a lot of particles are overlapping. This ring is however broader, and there are occasional spiral arms inside the ring (both trailing and leading features appear). The inner nuclear ring does not form in this model, which is not surprising since its size would be only few particle radii of this modified model.

3.2 Model II

Our second example is a three-dimensional model. As in Model I, the stellar disc is exponential, but now the initial value of the Toomre parameter is 1.5. The bulge mass is lower than in model I, 0.3×10^{10} $M_{\odot}$, and consequently the peak of the rotation curve, about 200 km s^{-1}, is also lower and its location is not determined by the bulge, but by the disc. The peak of the $\Omega - \kappa/2$ curve is higher than in Model I and the maximum occurs at smaller distance (0.5 versus 0.8 kpc in Model I) because the scalelength of the bulge is smaller being 0.3 kpc versus 0.6 kpc in Model I. There are again two modes (Fig. 5), which are in CR–ILR coupling, although the size of the secondary bar is smaller than in Model I. The coefficient of restitution, α, is 0.0.

The large-scale bar forms slowly in this model: between $T = 1.0$–2.5 Gyr an oval evolves to a bar, which grows and strengthens throughout the simulation. As can be seen from Fig. 6, there are two nuclear rings in Model II. The inner one, which forms first, follows closely the rotation of the secondary bar, whereas the outer one follows the primary bar or oval. Thus, the configuration of the double nuclear ring is opposite to that in Model I, where the inner one of the rings followed the primary bar. The outer nuclear ring in Model II is probably related to outer x_2 loops, which now extend deeper in the disc due to smaller size of the secondary bar. This ring shrinks by time, and eventually the two rings merge into a single very broad ring or gaseous disc, which occasionally exhibits spiral structure. The shrinking of the nuclear ring is fastest soon after its formation. At the same time, the primary bar component decelerates and becomes stronger.

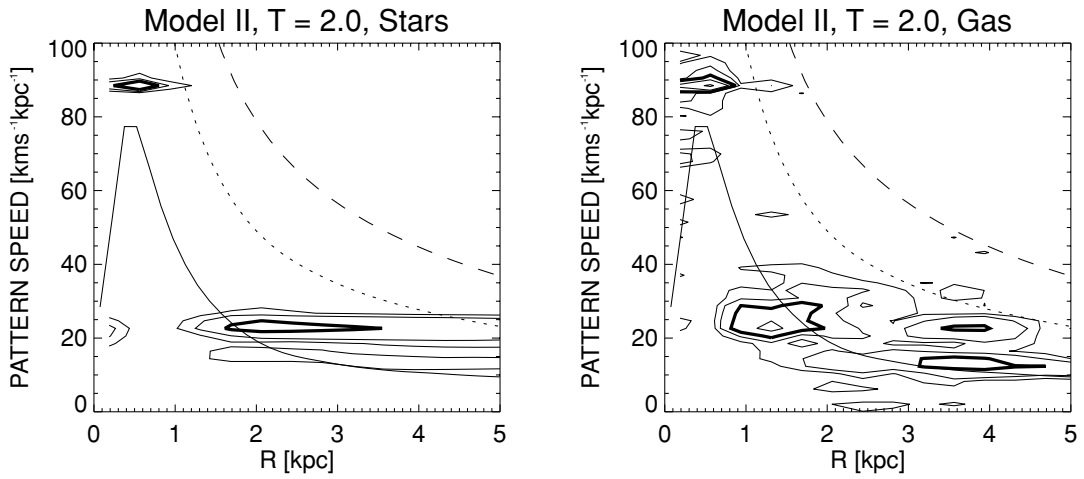

Figure 5. The $m = 2$ amplitude spectra of a double-barred Model II. The time interval used in the construction of the amplitude spectra is 1.5 Gyr centred at $T = 2.0$ Gyr. The contour levels are the same as in Fig. 1.

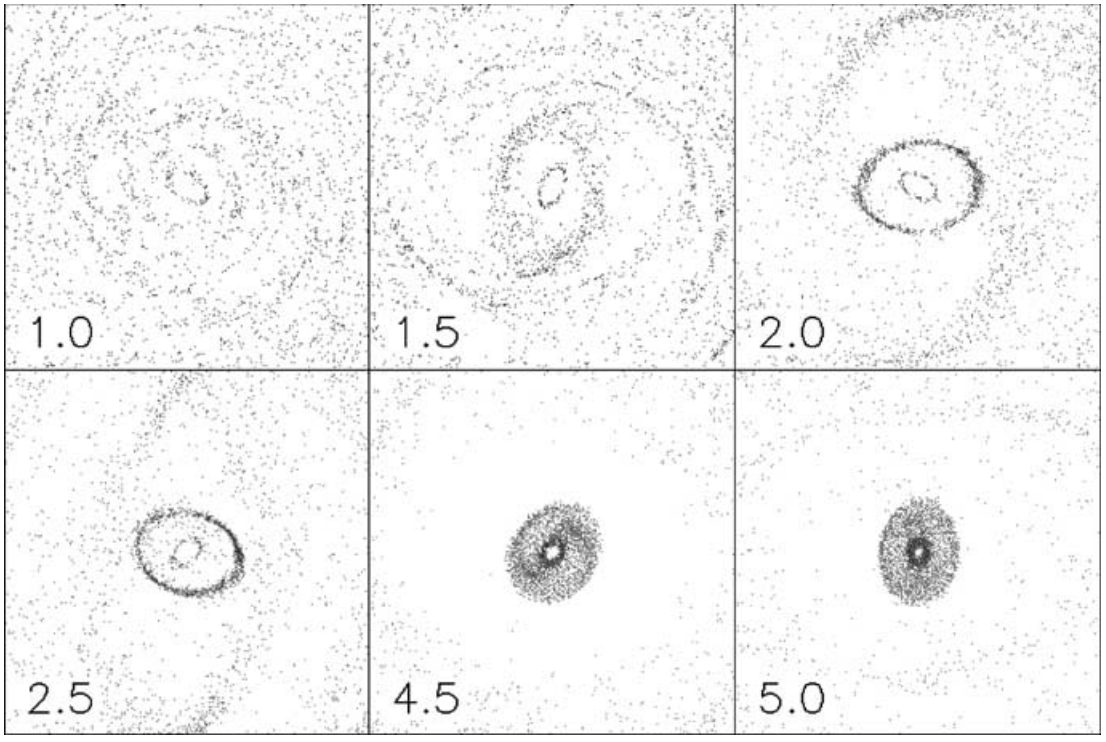

Figure 6. The evolution of the gas component in Model II. The width of the frame is 7.5 kpc. Time is shown in Gyr.

Note however, that this model does not include the star formation mechanism, and thus the particle density can reach such high values, that particles are overpacked, i.e. the distance between particle centres becomes smaller than the sum of the particle radii. The initial geometrical optical depth τ in this model is 0.04 and it can reach about 20 times higher values before particles start to overpack (at about $T = 2.0$ Gyr). We made variations of Model II, where we tried to avoid this problem by using smaller particle size or a simple star formation mechanism. Considerably reduced collision frequency leads to disappearance of the sharpest features, including the nuclear spiral. Also, the outer nuclear ring does not form (note that in the basic case it forms before overpacking starts to take place).

3.3 Model III

Unlike the previous models, Model III has a massive gas component: 95 per cent of the disc mass is in a stellar disc, whereas the remaining 5 per cent is in gas particles. The value of the Toomre parameter of the stellar disc is 1.5, and for the gas it is 1.0. The gas component is initially distributed as an exponential disc with scalelength of 6.75 kpc and the coefficient of restitution is 0.0. The masses and scalelengths of the disc and the bulge are the same as in Model II. Thus, the initial rotation curve is quite similar to that in Model II.

This model develops a large-scale bar even more slowly than Model II, only after $T = 4.0$ Gyr can a clear bar component be detected. The most interesting feature is the gaseous nuclear spiral

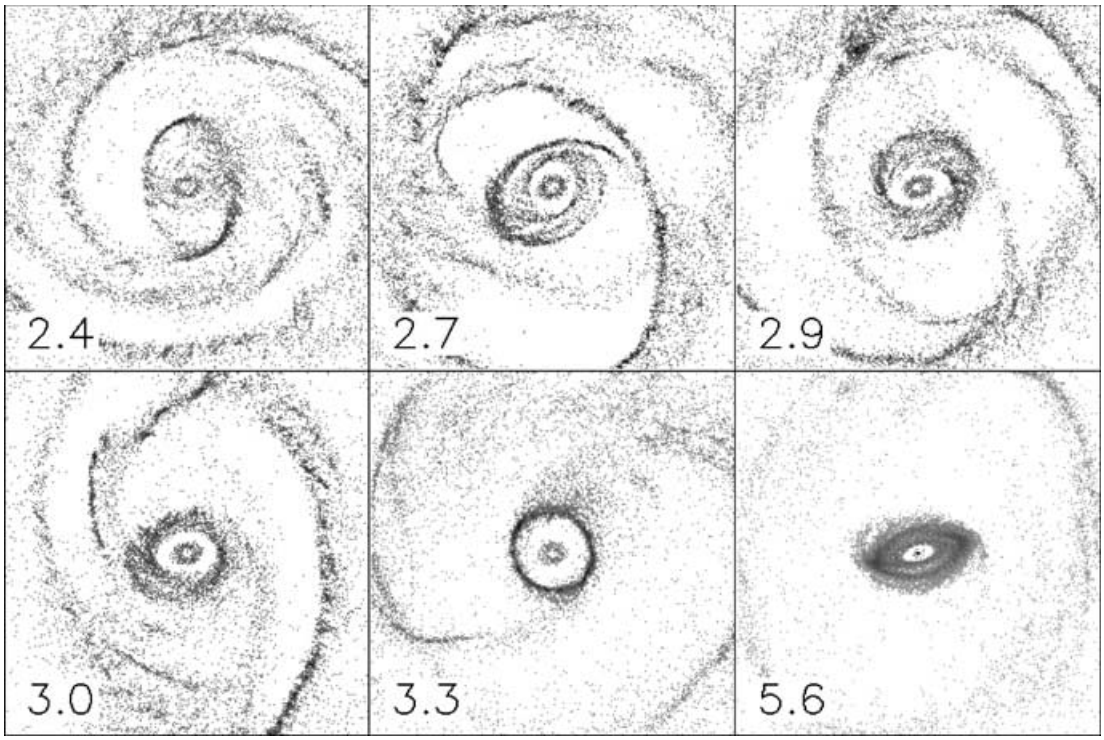

Figure 7. The evolution of the gas component in Model III. The width of the frames is 7.5 kpc. The contour levels of the amplitude spectra are the same as in Fig. 1 and the time is shown in Gyr.

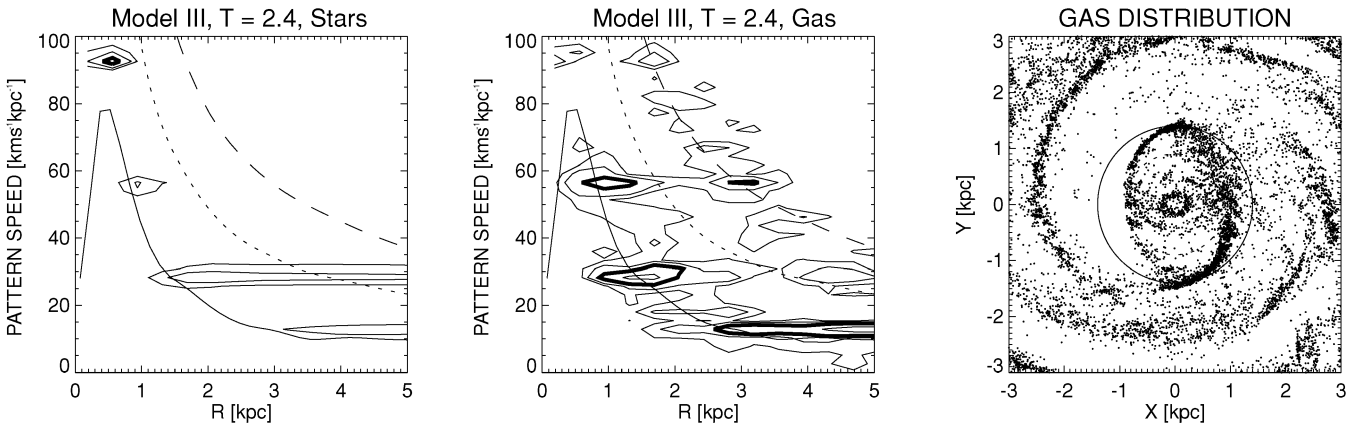

Figure 8. The $m = 2$ amplitude spectra of the stellar and the gas component and the gas distribution of Model III. The circle in the last frame shows the inner Lindblad radius (1.4 kpc) of the mode with pattern speed $\Omega_p \approx 30$ km s^{-1} kpc^{-1}. The contour levels of the amplitude spectra are the same as in Fig. 1.

structure, the morphology of which is changing (Fig. 7), forming occasionally a nuclear pseudoring. The $m = 2$ amplitude spectra at $T = 2.4$ Gyr (Fig. 8) show four modes. The mode with the highest pattern speed, $\Omega_p \approx 95$ km s^{-1} kpc^{-1}, is the only one that is also strong in the stellar component, and is well above the peak of the $\Omega - \kappa/2$ curve. The other modes, with pattern speeds $\Omega_p \approx 55$, 30 and 13 km s^{-1} kpc^{-1}, are much stronger in the gas component. Interestingly, in the stellar component, these modes tend to weaken at ILR, whereas in the gas component they can reach well inside the ILR. The nuclear spiral seems often to be connected to large-scale spiral, and occasionally one can 'follow' a spiral arm from 10 kpc scale down to 1 kpc scale. However, this is illusory: there is no mode with such a range. Later, a nuclear ring forms, and as in Model II, it eventually transforms to an elongated disc with a hole in the centre. There are spiral arms connecting the inner and outer edges of the nuclear disc. The elongated gas disc follows the rotation of a secondary stellar bar, or forms the gaseous part of the bar. The secondary bar can be in CR–ILR coupling with the main bar.

The nuclear region of Model III has serious problems with gas particle overpacking. This is owing to higher geometric optical depth, the initial value at one kpc from the centre is $\tau = 0.05$ and it reaches values well above unity when the nuclear spiral forms. Tests with lower level of dissipation usually led to disappearance of the inner gas spiral, and, for example, several concentric rings appeared. Model III is thus very sensitive to changes in gas particle parameters. This is understandable because the gas inflow also affects the gravitational potential, unlike our previous models.

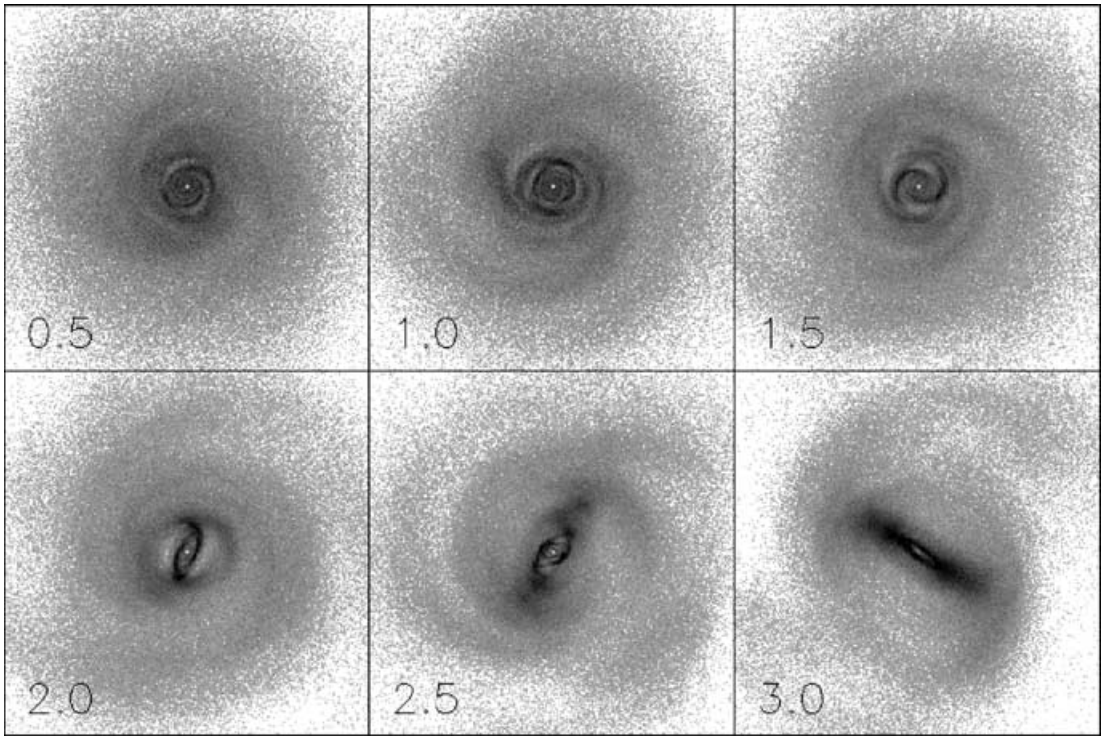

Figure 9. Model IV showing a stellar nuclear spiral. The width of the frame is 11.25 kpc. Time is shown in Gyr.

3.4 Model IV

In Model III the nuclear spiral arms were seen in the gas component, but the corresponding modes were very weak in the stellar component. However, we also have models where the nuclear spiral structure is strong in the stellar component. An example of this is Model IV, which has a strong halo component with mass $M_{\rm H} = 6.0 \times 10^{10}\ {\rm M}_{\odot}$. The disc mass is lower than in previous models, $M_{\rm D} = 4.8 \times 10^{10}\ {\rm M}_{\odot}$. The bulge is similar to that in Model I, and thus it is relatively more massive when compared with the disc, but its contribution to the total initial rotation curve is quite similar to that in Model I. Owing to a lower value of softening, the peak rotation velocity (about 235 km s^{-1}) is slightly higher than in Model I. The value of the initial Toomre parameter in this model is 1.25.

Fig. 9 shows the evolution of the stellar component in Model IV. The early evolution of this model is characterized by tightly wound nuclear spiral arms, which alternate between trailing and leading phases, occasionally forming ring-like structures. The gas component (not shown here) does not follow the spiral shape, instead it forms a ring around the alternating spiral. Similar recurrent nuclear spirals were present also in the simulations modelling M51 (Salo & Laurikainen 2000b). The explanation to alternating morphology is a reflection of individual trailing wave packets from the nucleus as leading packets. Although the pattern speeds of the wave packets are quite similar, producing a distinctive signal in the amplitude spectrum, owing to alternating morphology it is questionable whether this nuclear feature could be called a mode. The formation of a strong bar destroys the nuclear spirals in Model IV, as is also sometimes the fate of the secondary bars in our simulations. On the other hand, in a simulation with a hotter disc where bar formation was considerably delayed, these spirals can exist for several Gyr. This can also be the case when the large-scale bar is weak.

4 DISCUSSION

Our models show many features resembling those observed in the central region of barred and also some non-barred galaxies. Here we discuss the possible dynamical mechanisms behind the formation of such structures. We also discuss the star formation in the central region and gas inflow arising from non-axisymmetric perturbations. Finally, some limitations of our modelling approach are discussed.

4.1 Nuclear morphology and dynamics

Our models usually develop a fast-rotating central mode in the stellar component so that its pattern speed is originally above the peak of the $\Omega - \kappa/2$ curve. The rotation can later decelerate, but there are also examples where the central mode rotates steadily with its original high pattern speed. The first features or modes in the central parts of the systems are two-armed spirals, which may later evolve to secondary bars or nuclear rings. Naturally, the distinction between tightly wound spiral arms and a ring is subtle.

The further evolution of a central mode is affected by the formation of the primary bar. There are cases where the primary bar forms from the original central mode when its extent grows and its rotation rate decelerates from the original high value (see also Sellwood 1981). On the other hand, the primary bar can also form directly to a low pattern speed (well below the peak of the $\Omega - \kappa/2$ curve), and then the central mode and the primary bar can coexist. Two main scenarios can take place in our double-barred models: in the first case the secondary bar becomes part of the primary bar in less than 1 Gyr, and in the second case it can survive for several Gyr or to the end of the simulation.

The pattern speeds of modes in a stellar disc, e.g. the primary and secondary bars or bar and spiral arms, can depend on each other through non-linear mode coupling (Tagger et al. 1987; Masset &

Tagger 1997; Rautiainen & Salo 1999). This can happen when resonances of the two modes are overlapping, for example the ILR of the primary bar is roughly in the same radius as the corotation of the secondary bar. This ILR–CR resonance overlapping is common in our simulations, one example is Model I of this paper. However, we have not found this mode coupling necessary for the existence of two bars: in fact, in Papers I and II we have found other possible resonance overlappings including inner 4/1–CR, and at least one example in Paper II (model A2.5) seems to have no resonance overlapping at all: the OLR of the inner mode is inside the ILR of the outer mode.

A secondary bar rotating with a higher pattern speed than the primary bar is not the only possible mechanism behind complex central structure in galaxies. Friedli (1996) suggested that in gas-poor galaxies, secondary bars can be counter-rotating, if there are counter-rotating stars in the central region. The motivation of this model was the study by Friedli & Martinet (1993), according to which the prograde secondary bars required the presence of massive gaseous component. However, we have not found this necessary in this or previous studies (Papers I and II). On the other hand, with a series of simulations modulating the steepness of the rising part of the rotation curve by changing the scalelength or the mass of the analytical bulge, we found that the models with steeply rising rotation curves tend to have long-lasting central modes. The trend was similar both in disc and halo-dominated models. In the longest living double-barred case of Friedli & Martinet (1993), the secondary bar survived about five of its rotation periods. However, the frequency of secondary bars seems to be so high, at least 25 per cent of all barred galaxies (Erwin, Vega Beltrán & Beckman 2001b; Laine et al. 2002), that life-time of only five rotations seems unrealistic. So, either the secondary bars should be recurrent, or long-lived, as is the case in our models. Another difference to Friedli & Martinet (1993) is that in our models the secondary bar forms first or the two bars form at the same time, whereas in their models the primary bar formed first or the two bars appeared at the same time.

A very different scenario for the formation of a secondary bar was presented by Heller et al. (2001). In their model, there is only one analytical bar mode, which leads to a formation of a double nuclear ring near the ILR. These nuclear rings interacted hydrodynamically (self-gravity was neglected), and a very elongated nuclear ring or a secondary bar formed. This gaseous secondary bar rotated with a lower pattern speed than the primary bar. As in our Model I, the shape of this ring/bar depended on the relative orientation with respect to the primary bar, but the correlation was the opposite: the ring/bar was most elongated when it was parallel with the primary bar. Naturally, this difference is the result of very different dynamics behind these phenomena. In test particle simulations modelling IC 4214 (Salo et al. 1999), we found a phenomenon resembling the behaviour of the elongated nuclear ring in the model by Heller et al. (2001): the nuclear ring precessed occasionally, although there was only one pattern speed present in the potential. Also, in one of the models in Byrd et al. (1994) (model with the pattern speed $\Omega_{\rm p} = 0.05$ in simulation units, see their fig. 3) there was a very elongated nuclear ring that performed a swing-like motion around a parallel position with respect to the major axis of the bar potential. The mechanism suggested by Heller et al. can explain some of the observed gaseous secondary bars, but many secondary bars have strong stellar contribution, thus probably having a different origin.

The secondary bar in Model I is extremely long-lived, and it is accompanied by a very eccentric nuclear ring in the gas component. The cyclically changing shape of this ring can be easily explained by orbit loops found by Maciejewski & Sparke (2000): the nuclear ring follows the secondary bar, and it is most elongated when the two bars are perpendicularly aligned and roundest when they are parallel. The inner nuclear ring is always close to parallel alignment with the large-scale bar, and its shape does not change. There are also three distinctive radial regions in the amplitude spectrum of this model (see Fig. 1): the middle one (0.5–1.5 kpc) having a higher pattern speed than the primary bar, while the innermost one has the same pattern speed and also almost the same phase angle to the primary bar. All this is explained well if each feature is related to certain types of loops: the secondary bar and the outer nuclear ring are related to the inner x_2 loops, and the innermost stars and the inner nuclear ring are related to the inner x_1 loops. Interestingly, Erwin & Sparke (1999) report finding a triple bar in NGC 2681. The difference of the phase angles of the primary bar and the innermost bar is only 10°, which could mean that this galaxy represents a similar situation to our Model I. In Paper II we showed other examples of cyclic behaviour, but concerning outer and inner rings: in Model B2.25 the inner ring was usually misaligned with the bar, occasionally resembling the morphology of ESO 565-11. The major axis of the inner ring of this model seemed to follow a strong outer mode, and the shape of the ring depended on the relative orientation of the modes. There was also a secondary bar, and the nuclear ring of this model exhibits similar behaviour to the present Model I, but it was less prominent owing to lower ellipticity of the ring.

Double nuclear rings can form even in simulations with a single bar mode, usually so that the outer one is elongated perpendicularly with respect to the primary bar, while the quite round inner one is parallel with the bar (note however, that there are also examples of very elongated nuclear rings, which are parallel with primary bars). These two rings are located near the inner and outer ILRs. There are more double ring variations in models with two bars. In Model I, the outer nuclear ring follows the secondary bar and the inner nuclear ring follows the primary bar. In Model II the situation is the opposite, most likely owing to a slight decrease of the size of the secondary bar. Two nuclear rings can sometimes merge, and form a broad gaseous disc, with a hole in the centre. In a couple of such cases, the outer edge of the nuclear disc is rather round and elongated perpendicularly with respect to the primary bar, whereas the inner edge of the disc is more elongated and follows the secondary bar.

One suggested explanation for the observed nuclear spiral structures is that they are extensions of the gas response to a weak bar potential. Unlike the stellar density waves, the gas spiral can cross the inner Lindblad resonance (Englmaier & Shlosman 2000). In gas-dynamical simulations of Maciejewski et al. (2002) a spiral shock can extend inside a nuclear spiral/pseudoring in a single-bar model when the sound speed is high enough. This could be the case of the grand design nuclear structure of NGC 5248 (Laine et al. 2001), where the kinematics and the observed pitch angle suggest low pattern speed, and where neither large-scale nor nuclear bar are present. In our simulations, the mode with $\Omega_{\rm p} \approx 30\,{\rm km\,s^{-1}\,kpc^{-1}}$ in Model III could be example of this kind of behaviour: in the stellar component, the mode fades at the ILR, whereas in the gas component it is very strong even inside the ILR (see Fig. 8). Although this scenario is promising, it is not necessarily a universal mechanism behind nuclear morphology. For example, the continuity of the spiral structure to the central region is no proof of the presence of a single global mode: the isodensity contours in simulations with multiple modes often exhibit misleadingly continuous structure, distinctive gaps appearing only occasionally (Sellwood & Sparke 1988). Furthermore, strong non-linear perturbations in stellar components, such as bars, have no difficulty in crossing the ILR. Although most nuclear spirals have been detected only in gas or dust, there is the case of the

stellar nuclear spiral in M51, detected in the near-IR by Zaritsky, Rix & Rieke (1993). Tidal interaction models (Salo & Laurikainen 2000b) suggest that deeply penetrating spirals could be boosted by the inward propagation of the outer tidal waves.

Gasdynamical simulations (Knapen et al. 1995; Shlosman 1999) and analysis of damped orbits in a bar potential (Wada et al. 1994) have demonstrated that leading spiral-shaped features can form on the gas component near the inner ILR in the case of one bar with two ILRs. Knapen et al. (1995) studied the structure of M100, and concluded that the leading armlets seen in the near-IR are probably related to a young stellar population, thus probably being a gasdynamical phenomenon. Although the strong contribution of young stars seems probable in this case (Ryder & Knapen 1999), our Model IV and simulations by Salo & Laurikainen (2000b) show that transient leading central features are indeed also possible in the old stellar component.

It has also been suggested that some of the nuclear spirals could be formed by acoustic instabilities (Elmegreen et al. 1998; Elmegreen, Elmegreen & Eberwein 2002). The nuclear spiral structure formed by this mechanism would not be of grand design type, but could explain the flocculent nuclear structure in cases where the gas is only weakly self-gravitating and there is no stellar central mode.

4.2 Star formation and gas inflow

Many nuclear rings have enhanced star formation manifested as blue colours, H II-regions and concentrated molecular gas (see Buta & Combes 1996). In high-resolution images the star formation events can be seen often as hotspots or super star clusters (Maoz et al. 1996; Buta et al. 1999), whereas in some cases star formation is smoothly distributed along the nuclear ring (NGC 1326, Buta et al. 2000). The age estimates of the clusters in nuclear rings range from 1 to 300 Myr; older clusters may also exist, but they are not as easily detected as the young ones (Maoz et al. 2001). Some nuclear rings have a lot of dust (NGC 4151, Vila-Vilaro et al. 1995). There are also nuclear rings composed mainly of old stars (NGC 936, NGC 3945, NGC 4340, NGC 4371; Erwin et al. 2001b), possibly being remnants of previous star formation activity.

In Fig. 10 we show the gas distribution and stars formed in Model I. One can see that the ring of older stars still follows the rotation of the stellar secondary bar and accompanying gaseous nuclear ring in the sense that its major axis is almost parallel to the major axis of the gaseous nuclear ring. Later, the gaseous nuclear ring has become narrower, at least partly owing to a decrease in the number of gas particles caused by star formation. If the size of the gaseous nuclear ring gradually decreases, as often happens during the early evolutionary phases, the ring of older population of stars, which retains its original size (if orbits remain stable), can surround the gas ring. The gas clouds and new 'stars' in this simulation are massless, but at least one model with massive gas clouds and stars formed from them exhibits similar evolution.

The previously described behaviour could explain the observations of central structure of NGC 4314 (Combes et al. 1992), where the nuclear ring observed in molecular gas is smaller than that in the stellar component. NGC 4314 is also interesting because there are young stellar spiral arms outside the nuclear ring (Kenney et al. 1999), slightly resembling our Model III at $T = 5.6$ Gyr, where such features are present in the gas component (Fig. 7). In ESO 565-11 (Buta, Purcell & Crocker 1995), the size and also the orientation of the nuclear ring are wavelength-dependent. Based on a dynamical simulation constructed from an *H*-band image of this galaxy, Buta et al. (1999) suggest that the misalignment of the nuclear ring with respect to the bar is explained by the low age of the ring: later the ring becomes perpendicular with the bar.

A large-scale example of population-dependent ring morphology is IC 1438. In this galaxy the *B*-band morphology of the outer

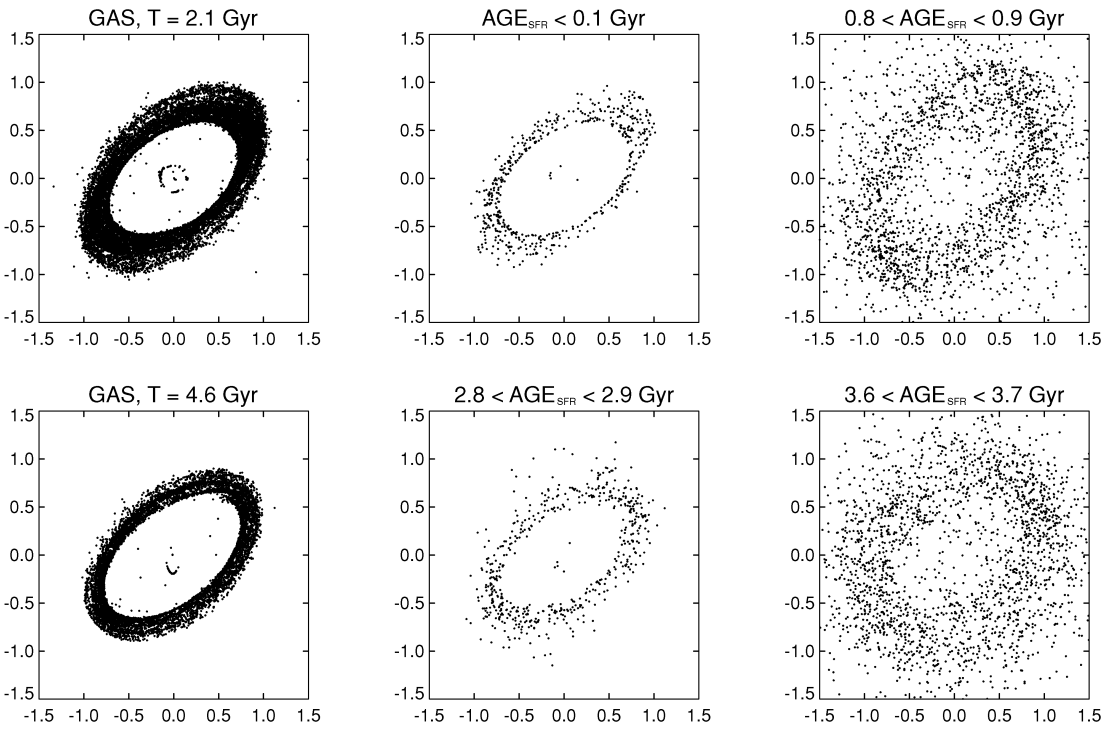

Figure 10. Star formation in the nuclear ring of Model I. In the top row, the left frame shows the gas distribution at $T = 2.1$ Gyr, the middle frame recently (age less than 100 Myr) formed stars, and the right frame stars formed at epoch $T = 1.2$–1.3 Gyr (age between 0.8 and 0.9 Gyr) from the beginning of the simulation. In the bottom row, the left frame shows the gas distribution at $T = 4.6$ Gyr, and the middle and the right frames the same stars as were shown in the top row.

pseudoring is R'_2, where the major axis of the pseudoring is parallel with the bar major axis, spiral arms winding 270°. On the other hand, the *I*-band morphology is R_1, where the major axis of the ring is perpendicular with respect to the bar major axis (Buta 1995). Byrd et al. (1994) suggested that this difference is related to evolution of the gas component: first having R_1 morphology, and then evolving to R'_2. Thus, the old stellar component would be a remnant of the past gas morphology, similar to fossil nuclear rings suggested by Erwin, Vega Beltrán & Beckman (2001a). As we demonstrated in Fig. 10, this is a possible scenario, but there is also another possibility, the evolution of the self-gravitating old stellar population. The outer ring morphology of one of our models in Paper II was very similar as in IC 1438, with outer rings of different subclasses in the stellar and the gas components. In the present study we have showed several examples, where the stellar component forms nuclear spirals and even pseudorings. Thus, it is tempting to speculate that some of the observed old population nuclear rings are not remnants of the earlier gas morphology, but instead have formed intrinsically in the old stellar disc itself. One possible example is NGC 3945, where the stellar nuclear ring shows spiral features (Erwin & Sparke 1999).

As has been known for more than 20 years, large-scale bars can drive gas inwards (for a short review, see e.g. Teuben 1996). It has been suggested that this inflow could feed activity in central regions of galaxies, either as starbursts or active galactic nuclei (AGN). Shlosman, Frank & Begelman (1989) suggested that there are nested bar components on smaller scales eventually feeding the nucleus. Although the connection between large-scale stellar bars and enhanced nuclear star formation seems established (Martinet & Friedli 1997; Aguerri 1999), there is no consensus about the possible connection between large-scale bars and active galactic nuclei. While some studies (Knapen, Shlosman & Peletier 2000; Laine et al. 2002) have found correlation, others have questioned it (McLeod & Rieke 1995; Moles, Marquez & Perez 1995; Ho, Filippenko & Sargent 1997; Mulchaey & Regan 1997; Hunt & Malkan 1999; Márquez et al. 2000). Furthermore, according to some recent studies active nuclei occur less frequently in galaxies with elongated bars (Shlosman, Peletier & Knapen 2000), and the galaxies with the strongest bars tend to be non-active (Laurikainen, Salo & Rautiainen 2002); in the latter study the bar strength was estimated directly from the maxima of the tangential to mean axisymmetric force ratios, following the suggestion by Buta & Block (2001).

There are some candidates of AGN fuelling induced by a secondary bar (Jogee, Kenney & Smith 1999; Colina & Wada 2000), but observations looking for features corresponding to the characteristic dust lanes in the leading edges of the large-scale bars with the *Hubble Space Telescope* (Regan & Mulchaey 1999) did not show any excess of secondary bars in Seyfert galaxies. However, one should not take this negative finding as a definitive answer yet. Athanassoula (1992) found that the presence of typical dust lanes in the leading side requires that the bar has an ILR and that it extends near the corotation resonance: the shape of the shock is related to change from x_1 orbits to x_2 orbits. Most secondary bars in our simulations rotate so rapidly that they do not have an ILR. Furthermore, these bars end well before reaching their corotation or even inner 4/1 radius, which agrees well with Maciejewski & Sparke (2000). Thus, the presence or absence of a secondary bar probably cannot be deduced from central dust lane morphology (see also Shlosman & Heller 2002).

In many of our models, the gas inflow stops at the nuclear ring, even though there is a secondary bar inside the ring. This is in agreement with the gasdynamical simulations of Maciejewski et al. (2002) showing that a realistic double-barred systems (in the sense that the orbits supporting the potential can be found) were not associated with strong gas inflow owing to lack of strong shocks. An interesting exception, where there is a lot of inflow of gas also inside a 1 kpc radius is our Model III, which includes self-gravitating gas. From the beginning to $T \approx 2$ Gyr the gas mass fraction inside a 1-kpc radius is more or less constant, about 1 per cent. When the nuclear spiral forms, the gas inflow starts, and at $T = 3$ Gyr the gas mass fraction of the disc is about 2 per cent. The inflow becomes strong after the formation of a large-scale bar (or maybe rather an oval), and so at $T = 3.5$ Gyr the gas mass fraction has reached 4.5 per cent. After this, the gas mass fraction is almost constant for about 1 Gyr. A second episode of strong inflow takes place at $T \approx 4.5$–5 Gyr when the gas mass fraction inside 1 kpc rises to 8.5 per cent of the stellar mass of the disc inside the same radius. This coincides with strengthening of the large-scale bar.

4.3 Limitations

Our models have several limitations. The method used to model the behaviour of the gas component is quite crude. The interstellar matter has several phases, and in addition to gravity and gasdynamical forces it is also affected by star formation, stellar winds and supernovae. These phenomena are especially strong in the nuclear regions of galaxies. In Paper II we tested the effect of star formation by making OB particles in collisions, and modelled also the consequent supernova explosions by giving velocity impulses to gas clouds near the OB particles after some time delay. With a suitable choice of parameters, it was possible to destroy all sharp features in the gas component, including nuclear rings. In the present study we studied the effect of dissipation by running our models with different values of the coefficient of restitution and gas particle sizes. Also, we made tests with and without the simple star formation procedure. These tests showed that the two nuclear rings of Model I are not very sensitive to level of dissipation or to the possible effects of particle overlaps. On the other hand, the nuclear spirals of Models II and III are more problematic. They seem to form only in very high dissipation cases where the density rises so high that particles are overpacked; the same simulations without overpacking, but also with a lower level of dissipation, can have e.g. concentric rings instead of nuclear spirals.

Gravity resolution of the simulations is also a problem. The smallest rings in our simulations, e.g. the innermost component of Model I, are comparable to the gravity softening length, and one should not expect these features to be properly modelled. Thus, our models do not have enough resolution to model the mass inflow close to an active galactic nucleus. On the other hand, many features have a size of several softening lengths, e.g. the diameter of the elongated nuclear ring in Model I is 5–6 ϵ. The resolution problems are not limited to simulations: the observed nuclear morphology of galaxies can depend strongly on the resolution of the images used.

5 CONCLUSIONS

Our main conclusions are as follows.

(1) Many nuclear features are affected by more than one mode, which can lead to rapidly changing nuclear morphology on a timescale of 10^7–10^8 yr.

(2) Double nuclear rings can form near two inner Lindblad resonances of a single mode, or can be related to two different modes.

(3) In a double-barred model, the evolution of an elongated nuclear ring can be understood by the concept of cyclic loops. Their influence can also be seen in the stellar component. This may be the first time that orbit loops have been clearly recognized in *N*-body models.

(4) Secondary bars, rings and spirals can form in both the stellar and the gas components. Thus it is unclear whether stellar nuclear rings are relics of earlier gaseous morphology or active evolution of the old stellar population. Also, some of the observed near-IR nuclear spirals can be related to the old stellar population.

(5) Secondary bars in our models are often destroyed by becoming part of the primary bar, but there are also examples with lifetimes of several Gyr. The high frequency of double-barred galaxies suggest that they can be long-lived.

(6) Gaseous nuclear spirals appear in our simulations when the level of dissipation is very high. However, in such models the gas particles are overpacked owing to limitations of the method we have used in modelling the interstellar gas.

(7) Gas inflow along the large-scale bars is often stopped in the nuclear ring. There can also be inflow related to a gaseous nuclear spiral, but it is much weaker than in the case of a large-scale bar. On the other hand, secondary bars in our simulations seem not to be connected with considerable gas inflow. This, however, needs to be checked with better resolution simulations.

ACKNOWLEDGMENTS

We thank the referee, Dr P. Englmaier, for his comments that helped to improve the manuscript. This work has been supported by Wihuri and Väisälä foundations and by the Academy of Finland.

REFERENCES

Aguerri J. A. L., 1999, A&A, 351, 43
Athanassoula E., 1992, MNRAS, 259, 345
Burbidge E., Burbidge G. R., 1960, ApJ, 132, 30
Buta R., 1995, ApJS, 96, 39
Buta R., Block D. L., 2001, ApJ, 550, 243
Buta R., Combes F., 1996, Fundam. Cosmic Phys., 17, 95
Buta R., Purcell G. B., Crocker D. A., 1995, AJ, 110, 1588
Buta R., Crocker D. A., Byrd G. G., 1999, AJ, 118, 2071
Buta R., Treuthardt P. M., Byrd G. G., Crocker D. A., 2000, AJ, 120, 1289
Byrd G., Rautiainen P., Salo H., Buta R., Crocher D. A., 1994, AJ, 108, 476
Carollo C. M., Stiavelli M., de Zeeuw P. T., Mack J., 1997, AJ, 114, 2366
Colina L., Wada K., 2000, ApJ, 529, 845
Combes F., Gerin M., Nakai N., Kawabe R., Shaw M. A., 1992, A&A, 259, L27
Contopoulos G., Grosbøl P., 1989, A&AR, 1, 261
Elmegreen B. G. et al., 1998, ApJ, 503, L119
Elmegreen D. M., Elmegreen B. G., Eberwein K. S., 2002, ApJ, 564, 234
Englmaier P., Shlosman I., 2000, ApJ, 528, 677
Erwin P., Sparke L. S., 1999, ApJ, 521, L37
Erwin P., Vega Beltrán J. C., Beckman J., 2001a, Ap&SS Suppl., 277, 457
Erwin P., Vega Beltrán J. C., Beckman J. E., 2001b, in Knapen J. H., Beckman J. E., Shlosman I., Mahoney T. J., eds, ASP Conf. Ser. Vol. 249, The Central Kiloparsec of Starbursts and AGN: The La Palma Connection. Astron. Soc. Pac., San Franscisco, p. 171
Friedli D., 1996, A&A, 312, 761
Friedli D., Martinet L., 1993, A&A, 277, 27
Friedli D., Wozniak H., Rieke M., Martinet L., Bratschi P., 1996, A&AS, 118, 461
Heller C. H., Shlosman I., Englmaier P., 2001, ApJ, 553, 661
Ho L. C., Filippenko A. V., Sargent W. L. W., 1997, ApJ, 487, 591
Hunt L. K., Malkan M. A., 1999, ApJ, 516, 660
Jogee S., Kenney J. D. P., Smith B. J., 1999, ApJ, 526, 665
Kenney J. D. P., Friedli D., Benedict G. F., Leon S., Combes F., 1999, in Merritt D., et al., eds, ASP Conf. Ser. Vol. 182, Galaxy Dynamics – A Rutgers Symposium. Astron. Soc. Pac., San Francisco, 235
Knapen J. H., Beckman J. E., Heller C. H., Shlosman I., de Jong R. S., 1995, ApJ, 454, 623
Knapen J. H., Shlosman I., Peletier R. F., 2000, ApJ, 529, 93
Laine S., Knapen J. H., Perez-Ramirez D., Englmaier P., Matthias M., 2001, MNRAS, 324, 891
Laine S., Shlosman I., Knapen J. H., Peletier R. F., 2002, ApJ, 567, 97
Laurikainen E., Salo H., Rautiainen P., 2002, MNRAS, 331, 880
Maciejewski W., Sparke L. S., 1997, ApJ, 484, L117
Maciejewski W., Sparke L. S., 2000, MNRAS, 313, 745
Maciejewski W., Teuben P. J., Sparke L. S., Stone J. M., 2002, MNRAS, 329, 502
Maoz D., Barth A. J., Sternberg A., Filippenko A. V., Ho L. C., Macchetto F. D., Rix H., Schneider D. P., 1996, AJ, 111, 2248
Maoz D., Barth A. J., Ho L. C., Sternberg A., Filippenko A. V., 2001, AJ, 121, 3048
Márquez I. et al., 2000, A&A, 360, 431
Martinet L., Friedli D., 1997, A&A, 323, 363
Masset F., Tagger M., 1997, A&A, 322, 442
McLeod K. K., Rieke G. H., 1995, ApJ, 441, 96
Moles M., Marquez I., Perez E., 1995, ApJ, 438, 604
Mulchaey J. S., Regan M. W., 1997, ApJ, 482, L135
Rautiainen P., Salo H., 1999, A&A, 348, 737
Rautiainen P., Salo H., 2000, A&A, 362, 465
Regan M. W., Mulchaey J. S., 1999, AJ, 117, 2676
Ryder S. D., Knapen J. H., 1999, MNRAS, 302, L7
Salo H., 1991a, A&A, 243, 118
Salo H., 1991b, Icarus, 90, 254
Salo H., 1992, Nat, 359, 619
Salo H., Laurikainen E., 1993, ApJ, 410, 586
Salo H., Laurikainen E., 2000a, MNRAS, 319, 377
Salo H., Laurikainen E., 2000b, MNRAS, 319, 393
Salo H., Rautiainen P., Buta R., Purcell G. B., Cobb M. L., Crocker D. A., Laurikainen E., 1999, AJ, 117, 792
Sandage A., 1961, The Hubble atlas of galaxies. Carnegie Inst., Washington
Sellwood J. A., 1981, A&A, 99, 362
Sellwood J. A., 1987, ARA&A, 25, 151
Sellwood J. A., Sparke L. S., 1988, MNRAS, 231, 25
Shlosman I., 1999, in Beckman J. E., Mahoney T. J., eds, ASP Conf. Ser. Vol. 187, The evolution of Galaxies on Cosmological Time-scales. Astron. Soc. Pac., San Francisco, p. 100
Shlosman I., Heller C. H., 2002, ApJ, 565, 921
Shlosman I., Frank J., Begelman M. C., 1989, Nat, 338, 45
Shlosman I., Peletier R. F., Knapen J. H., 2000, ApJ, 535, L83
Tagger M., Sygnet J. F., Athanassoula E., Pellat R., 1987, ApJ, 318, L43
Teuben P., 1996, in Buta R., et al., eds, ASP Conf. Ser. Vol. 91, IAU Colloq. 157, Barred Galaxies. Astron. Soc. Pac., San Francisco, p. 299
Vila-Vilaro B. et al., 1995, A&A, 302, 58
Wada K., Taniguchi Y., Habe A., Hasegawa T., 1994, ApJ, 437, L123
Wozniak H., Friedli D., Martinet L., Martin P., Bratschi P., 1995, A&AS, 111, 115
Zaritsky D., Rix H., Rieke M., 1993, Nat, 364, 313

This paper has been typeset from a TEX/LATEX file prepared by the author.